Journal of Materials Chemistry C

Accepted Manuscript

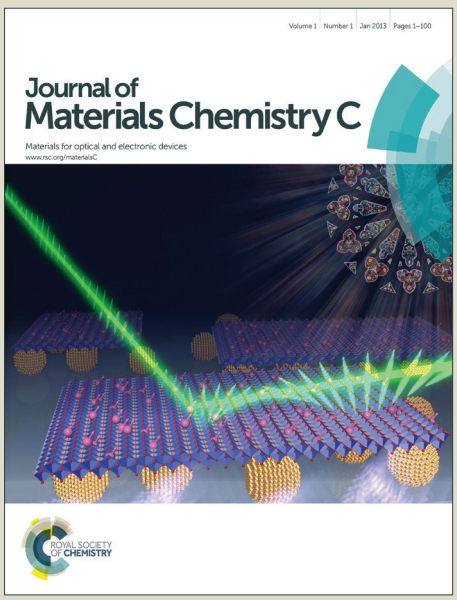

This is an *Accepted Manuscript*, which has been through the Royal Society of Chemistry peer review process and has been accepted for publication.

Accepted Manuscripts are published online shortly after acceptance, before technical editing, formatting and proof reading. Using this free service, authors can make their results available to the community, in citable form, before we publish the edited article. We will replace this *Accepted Manuscript* with the edited and formatted *Advance Article* as soon as it is available.

You can find more information about *Accepted Manuscripts* in the Information for Authors.

Please note that technical editing may introduce minor changes to the text and/or graphics, which may alter content. The journal's standard Terms & Conditions and the Ethical guidelines still apply. In no event shall the Royal Society of Chemistry be held responsible for any errors or omissions in this *Accepted Manuscript* or any consequences arising from the use of any information it contains.

ROYAL SOCIETY OF CHEMISTRY

www.rsc.org/materialsC

Journal Name

ARTICLE

Solution-processed bulk heterojunction solar cells based on porphyrin small molecules with very low energy losses comparable to perovskite solar cells and high quantum efficiencies

Received 00th January 20xx,
Accepted 00th January 20xx

DOI: 10.1039/x0xx00000x

www.rsc.org/

Ke Gao[a], Liangang Xiao[a], Yuanyuan Kan[a], Binglin Yang[a], Junbiao Peng[a], Yong Cao[a], Feng Liu*[b], Thomas Russell[c] and Xiaobin Peng*[a]

Two new A-D-A conjugated small molecules **Por-Rod** and **Por-CNRod** are developed using a porphyrin core as the donor unit and 3-ethylrhodanine and 2-(1,1-dicyanomethylene)rhodanine as the acceptor units. **Por-Rod** and **Por-CNRod** show broad absorptions to ~850 nm with optical energy band gap of 1.47 and 1.45 eV, and their blend films with $PC_{71}BM$ show SCLC hole mobilities of 8.5×10^{-5} and 7.5×10^{-6} $cm^2 V^{-1} s^{-1}$, respectively. Though their bulk heterojunction solar cells with $PC_{71}BM$ processed without additive, only with thermal annealing or only with pyridine additive show very low power conversion efficiencies (PCEs), the **Por-Rod**-based solar cells processed with pyridine and then thermal annealing show a PCE up to 4.97% with a remarkable V_{OC} up to 0.94 V, showing a very low energy loss of only 0.53 eV. This is the first report that small molecule-based solar cells show such a low energy loss comparable to perovskite solar cells but with a good PCE of about 5% and a maximum external quantum efficiency up to 61%. To further understand the effect of different processing conditions on the blend films, the morphology of their blend films is studied by grazing incidence X-ray diffraction and resonant soft X-ray scattering.

Introduction

Solution processed organic photovoltaic has been deemed to be a good solution to the imminent shortage, the rising prices and the relating environmental problems of fossil fuels because of their low cost, lightweight, and mechanical flexibility.[1-5] Also great progresses have been achieved during the past decade,[6-11] with the power conversion efficiencies (PCEs) over 10% for single bulk heterojunction (BHJ) organic solar cells (OSCs) based on both polymers and small molecules (SMs).[12-18] Compared to polymers, SMs cannot only enrich the material choices, but also show the advantages such as defined molecular structures, definite molecular weights, easy purification and good batch-to-batch reproducibility, which are more suitable for the commercialization of OSCs.[7, 19-23]

On the other hand, recent years also have witnessed the unprecedentedly rapid progress of perovskite solar cells.[24, 25] Compared with perovskite solar cells, the main issue of present OSCs is how to obtain a high open circuit voltage (V_{OC}) and a short circuit current (J_{sc}) simultaneously.[2, 26-30] Firstly, it is impossible to convert the whole energy bandgap (E_g) of the donor material to V_{OC} because driving forces are needed between the donor and acceptor materials in OSCs. A key parameter of the energy loss (E_{loss}), which defines as $E_{loss}=E_g - eV_{OC}$, create a link between the V_{OC} and the E_g, and the minimum E_{loss} was suggested to be 0.6 eV for efficient BHJ OSCs.[30] Secondly, though the E_{loss} below 0.6 eV sometimes can be achieved for OSCs, the external quantum efficiency (EQE) drops remarkably because a too low E_{loss} enhances the charge recombination significantly even though a lower E_{loss} can also help the charge separation.[28] On the contrary, the E_{loss} values can be low to 0.5-0.55 eV but still with very high EQE for perovskite solar cells.[25, 31] Therefore to lower the E_{loss} values comparable perovskite solar cells but still maintaining high EQE is important to further improve the performance of BHJ OSCs.[7] However, most BHJ OSCs show energy losses above 0.7 eV, and the OSCs with energy losses below 0.6 eV usually show low EQE values as show in Figure 1.[7, 24, 28, 29, 32] Although there are many ways to reduce the energy losses and obtain high Voc values such as: (1) tuning the energy levels of donor materials, (2) increasing crystallinity without decreasing D/A interfaces to provide more paths for charge separation,[33] (3) reducing the exciton binding energy and getting a higher E_{eff} by increasing the permittivity,[34] and (4) lowing bimolecular non-

[a] State Key Laboratory of Luminescent Materials and Devices, South China University of Technology, 381 Wushan Road, Guangzhou, 510640, P. R. China *Email：chxbpeng@scut.edu.cn.
[b] Materials Sciences Division, Lawrence Berkeley National Lab, Berkeley, CA, 94720, USA *Email：iamfengliu@gmail.com.
[c] Polymer Science and Engineering Department, University of Massachusetts, Amherst, MA 01003, USA

† Footnotes relating to the title and/or authors should appear here.
Electronic Supplementary Information (ESI) available: [details of any supplementary information available should be included here]. See DOI: 10.1039/x0xx00000x

Journal of Materials Chemistry C Accepted Manuscript

Please do not adjust margins

radiative recombination,[35] it is still not easy to obtain a low energy loss but with high EQE values for BHJ solar cells.

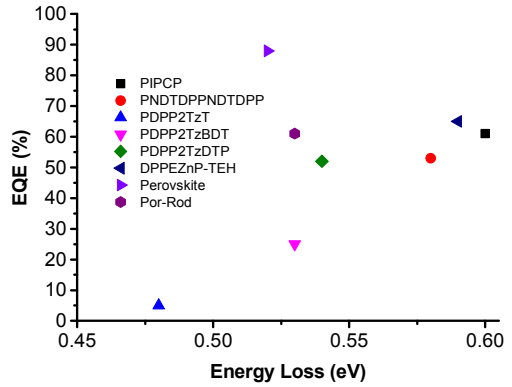

Figure 1. Maximum EQE vs the energy loss for published donors with low energy loss below 0.6 eV.

Porphyrins and their derivatives have been studied as the active materials in initial OPV studies because of the easy modifications of the periphery or by metal insertion into the cavity, extensively π-conjugated systems and high molar absorption coefficients.[36-38] Very recently, we developed conjugated donor-acceptor-donor (A-D-A) porphyrin small molecules, in which electron-deficient units were linked to the electron-rich porphyrin core through ethynylene, for solution-processed BHJ OSCs, and the PCEs were finally enhanced up to 8%.[7] Considering the good performance of the electron-deficient units of 3-ethylrhodanine and 2-(1,1-dicyanomethylene)rhodanine in OPV molecules,[39-41] herein, we design and prepare two new A-D-A SMs of **Por-Rod** and **Por-CNRod**, in which 3-ethylrhodanine and 2-(1,1-dicyanomethylene)rhodanine units, respectively, are symmetrically conjugated through thiophenylethynyl bridges to a porphyrin core for BHJ OSCs.[42, 43] We not only explore the photovoltaic properties of the BHJ OSCs based on them as the donor materials but also the morphology of the blend films under different device fabrication conditions.

Experimental

General methods

^{1}H NMR spectra were conducted on a Bruker AVANCE Digital 300 MHz spectrometer in deuterated chloroform using tetramethylsilane as an internal standard. Mass Spectrometry (MS) data were obtained on a Bruker Daltonics BIFLEX III MALDI-TOF Analyzer using MALDI mode. UV-vis-NIR absorption spectra of the films on quartz substrates were measured using a Shimadzu UV-3600 spectrophotometer. Photoluminescence spectra were recorded on a Horiba Fluoromax-4 spectrofluorometer. Cyclic voltammetry (CV) was carried out on a CHI660A electrochemical workstation with platinum electrodes at a scan rate of 50 mV s^{-1} against an Ag/AgCl reference electrode and ferrocene/ferrocenium (Fc/Fc+) as the internal potential standard with nitrogen-saturated solution of 0.1 M tetrabutylammonium hexafluorophosphate (Bu_4NPF_6) in chloroform. The *J-V* characteristics were measured under AM 1.5 solar simulator (Japan, SAN-EI, XES-40S1) at 100 mW cm^{-2} calibrated with a standard Si solar cell, and the data were collected using a Keithley 2400 digital source meter.

Synthesis of Por-Rod and Por-CNRod

All operations including air-sensitive reagents were conducted under an inert atmosphere of nitrogen or argon. All chemicals and solvents were used as received unless otherwise indicated from commercial sources (TCI, Sigma Aldrich, J&K, Alfa Aesar). Toluene, tetrahydrofuran (THF) and triethylamine were all dried by distillation over sodium prior to use. Rhodanine-$(CN)_2$ was synthesized according to reported procedures,[39] and the detailed synthetic procedures of **6** are shown in supporting information. The main synthetic routes of **Por-Rod** and **Por-CNRod** are shown in Scheme 1. The chemical structures of **Por-Rod** and **Por-CNRod** were confirmed by ^{1}H NMR, MALDI-TOF mass spectroscopy and elemental analysis.

Compound 4

40 mL acetic acid was added to the mixture of **1** (546.7 mg, 2.862 mmol) and **2** (506.9 mg, 3.148 mmol) under argon before ammonium acetate (484.8 mg, 6.297 mmol) was added. After stirred and heated at 110 ℃ for 36 h, the mixture was extracted with CH_2Cl_2, washed with water and dried over anhydrous Na_2SO_4. After the removal of solvent, the crude product was first purified by column chromatography and then recrystallized from CH_2Cl_2 and CH_3OH to afford **4** as a yellow solid (915 mg, 96%). ^{1}H NMR (300 MHz, $CDCl_3$) δ (ppm): 7.75 (s, 1H), 7.16 (d, 2H), 4.18 (q, 2H), 1.29 (t, 3H).

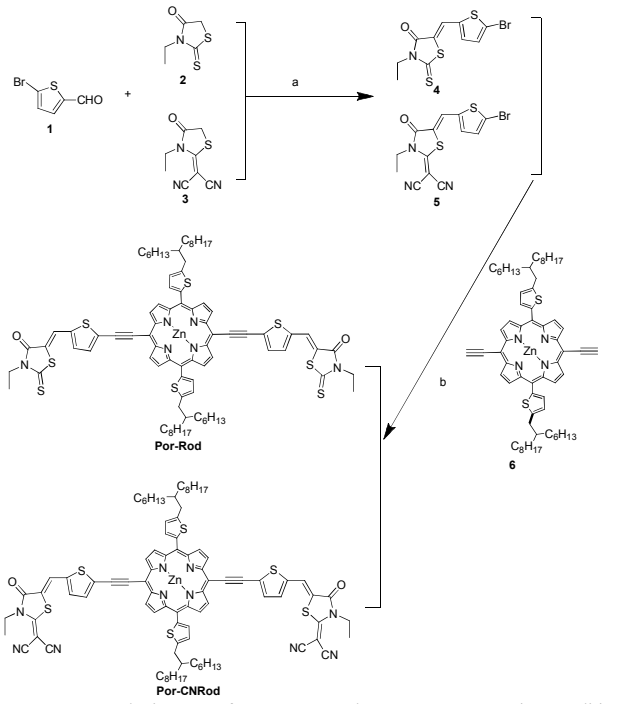

Scheme 1. Synthetic routes for **Por-Rod** and **Por-CNRod**. Reaction condition: (a) ammonium acetate/acetic acid for aldol condensation reaction reactions; (b) $Pd(PPh_3)_4$/CuI, toluene/triethylamine for Sonogashira reaction coupling reactions.

This journal is © The Royal Society of Chemistry 20xx

Please do not adjust margins

Journal of Materials Chemistry C Accepted Manuscript

Compound 5

Similar procedures as the synthesis of **4** but with **3** as one of the starting materials to afford **5** as a light yellow solid (yield: 90%). ^{1}H NMR (300 MHz, $CDCl_3$) δ (ppm): 7.96 (s, 1H), 7.24 (d, 1H), 7.21 (d, 1H), 4.34 (q, 2H), 1.39 (t, 3H).

Por-Rod

To a 50 mL two necked round-bottom flask were added compound **6** (103.3mg, 0.1 mmol), **4** (99.9 mg, 0.3 mmol), anhydrous toluene (12 mL) and triethylamine (6 mL), and the mixture was deoxygenated with Ar for 30 min before $Pd(PPh_3)_4$ (11.55 mg, 0.01mmol) and CuI (1.9 mg, 0.01mmol) were added. Then the mixture was stirred at 80 ℃ for 72 h under the protection of Ar. After cooled to room temperature, the mixture was washed with water and dried over anhydrous Na_2SO_4. Then the solvent was removed, and the residue was purified by column chromatography to give a black solid **Por-Rod** (yield: 77%). Mass (MALDI-TOF): Obs. 1539.6; Calcd. for $C_{84}H_{94}N_6O_2S_8Zn$, 1538.4. Anal. Calcd. for $C_{84}H_{94}N_6O_2S_8Zn$: C, 65.45; H, 6.15; N, 5.45. Found: C, 65.29; H, 6.28; N, 5.39.

Por-CNRod

Similar procedures as the synthesis of **Por-Rod** but with **5** as one of the starting materials to afford **Por-CNRod** as a black solid (yield: 75%). Mass (MALDI-TOF): Obs. 1604.1; Calcd. for $C_{90}H_{94}N_{10}O_2S_6Zn$, 1602.5. Anal. Calcd. for $C_{90}H_{94}N_{10}O_2S_6Zn$: C, 67.33; H, 5.90; N, 8.72 . Found: C, 66.83; H, 6.03; N, 8.68.

Results and discussion

Synthesis of Por-Rod and Por-CNRod

Two new A-D-A porphyrin organic semiconductor materials are synthesized. The aldol condensation reaction of commercially available **1** with **2** or **3** produced compound **4** or **5**. The bis-Sonogashira reaction of **4** or **5** with **6** affords the target product **Por-Rod** or **Por-CNRod** in good yield about 75%. More important, no toxic tin compound or dangerous lithium reagent was used in the whole synthetic routes.[7]

Optical and electrochemical properties

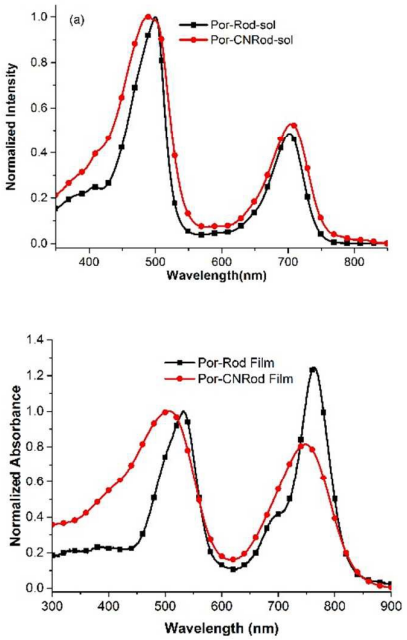

Figure 2. UV-vis-NIR absorption spectra of **Por-Rod** and **Por-CNRod** (a) in THF solutions and (b) in films.

Figure 1 shows the UV-vis-NIR absorption spectra of **Por-Rod** and **Por-CNRod** in very dilute THF solution and thin film cast from chlorobenzene (CB) solution, and the corresponding optical properties including the absorption edges (λ_{onset}), absorption peaks (λ_{max}), and optical bandgaps (E_g^{opt}) are summarized in Table 1. **Por-Rod** in THF exhibits two absorption peaks at 500 and 703 nm, which are ascribed to the Soret band and Q band of porphyrin, respectively. The strong and red-shifted Q band than normal non-functionalized porphyrins indicates that there is strong intramolecular charge transfer.[37] On the other hand, **Por-CNRod** shows quite similar absorption profile but with a slightly blue-shifted and broaden Soret band. **Por-Rod** and **Por-CNRod** films cast from CB exhibit remarkably intensified NIR absorption peaks to 764 and 748 nm, respectively. The more intensified and longer wavelength shifted NIR absorption peak of **Por-Rod** indicate the stronger *J*-aggregation of **Por-Rod** than **Por-CNRod** in the solid state.[44] The optical band gaps estimated from the onset absorption edges are 1.47 eV and 1.45 eV for **Por-CN** and **Por-CNRod**, respectively.

Table 1 Optical and electrochemical data for Por-Rod and Por-CNRod.

Donor	λ_{max}/nm (solution)	λ_{onset}/nm (film)	E_{ox} [V]	E_{HOMO} [eV]	E_{LUMO} [eV]	E_g^{opt}[eV][a]
Por-Rod	500	843	0.44	-5.24	-3.77	1.47
Por-CNRod	488	854	0.52	-5.32	-3.87	1.45

[a] Optical band gap estimated from the formula of $1240/\lambda_{onset}$, and λ_{onset} is the onset of the absorption spectrum in film.

Journal of Materials Chemistry C Accepted Manuscript

Please do not adjust margins

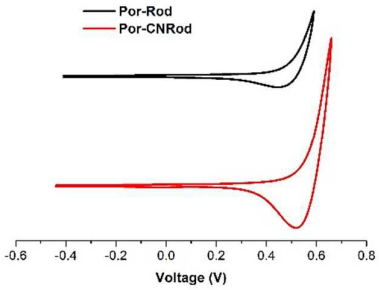

Figure 3. Cyclic voltammogram of **Por-Rod** and **Por-CNRod** with Ag/Ag^+ electrode as the reference and an energy level of ferrocene of 4.80 eV as the internal standard.

The electrochemical properties of the two molecules were investigated by CV in order to obtain the frontier orbit energy levels. HOMO energy levels (E_{HOMO}) are estimated according to the empirical equation of $E_{HOMO} = -(4.8 + E_{ox})$, where E_{ox} is the onset oxidation potential of molecules relative to that of Fc/Fc^+ standard. As shown in Figure 2, $E_{ox(Por\text{-}Rod)}$ and $E_{ox(Por\text{-}CNRod)}$ after the deduction of $E_{ox(Fc/Fc+)}$ were measured to be 0.44 and 0.48 V, thus the HOMO energy levels are calculated to be −5.24 and -5.32 eV, and the LUMO energy levels (E_{LUMO}) are calculated to be -3.77 and -3.87 eV for **Por-Rod** and **Por-CNRod**, respectively, according to $E_{LUMO} = E_{HOMO} + E_g^{opt}$. Their electrochemical data and the HOMO and LUMO energy levels are summarized in Table 1.

Photovoltaic properties and exciton dissociation rate

The solution-processed BHJ OSCs were fabricated with $PC_{71}BM$ as the electron acceptor and **Por-Rod** or **Por-CNRod** as the electron donor in a conventional device structure of ITO/PEDOT:PSS/BHJ blends/PFN/Al (ITO: indium tin oxide; PEDOT:PSS: poly(styrene sulfonate)-doped poly(ethylene-dioxythiophene); PFN: poly[(9,9-bis(30-(N,N-dimethylamino)propyl)-2,7-fluorene)-alt-2,7-(9,9-dioctylfluorene)]) under different conditions, and then measured under AM 1.5 illumination. The ratio of **Por-Rod** or **Por-CNRod** to $PC_{71}BM$ was optimized to be 1:1 (w/w). Device results are summarized in Table 2, and their corresponding J-V curves are shown in Figure 3 and Figure S1. All the OSCs fabricated just using CB as the solvent without any post treatment show very poor performance. And the addition of pyridine (Py) additive (1 v%), which was often used to improve the film morphology of zinc(II) porphyrins, only improves the device performance slightly. However, it is noted that Py additive can enhance the V_{OC}. Especially, the **Por-CNRod**-based OSCs show a high V_{OC} up to 0.94 V. Since the E_g of **Por-CNRod** is 1.45 eV, the E_{loss} for **Por-CNRod**-based OSCs fabricated with Py additive is just 0.51 eV, which is smaller than the 0.55 eV value for perovskite solar cells when PEDOT:PSS is used.[31] Therefore, the V_{OC} is very high for such a small bandgap molecule-based OSCs. However, the small J_{sc} and FF lead to a poor PCE of only 0.6%.

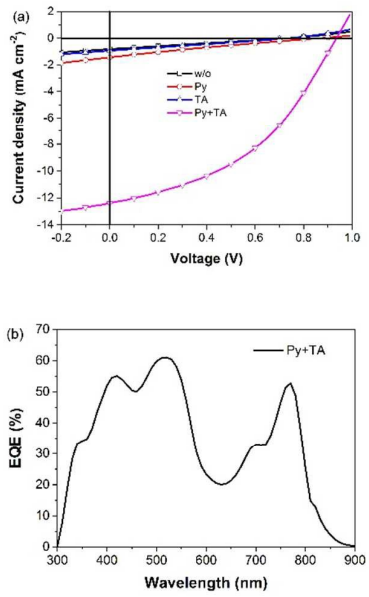

Figure 4. *J–V* curves (a) and EQE (b) of the OSCs with the device structure of ITO/PEDOT:PSS/**Por-Rod**:$PC_{71}BM$ (1:1, w/w)/PFN/Al.

Thermal annealing does not take effects for these OSCs either, inducing similar or inferior performance to those fabricated without any post treatments. However, when the devices were further optimized with Py additive and then thermal annealing, **Por-Rod**-based devices exhibit a significant PCE enhancement up to 4.97 % with a J_{sc} of 12.39 mA/cm^2, a fill factor of 42.71 % and a V_{OC} of 0.94 V while **Por-CNRod**-based ones do not show an improved performance. The V_{OC} values of the OSCs changes obviously under different device fabrication conditions, showing that film morphology impacts significantly on the open-circuit voltages.[45, 46] As show in Table 2, the *Voc* values for the devices fabricated with pyridine additive are increased compared with those without pyridine, which can be ascribed to the more D/A interfaces induced by pyridine.[35] On the other hand, different device fabrication conditions can lead to different degree of crystallinity and more disorder morphology introduces a broad distribution of energy states of the electronic carriers to penalize energy output by enhanced recombination, which reduces the photo-voltages.[33] Therefore, more D/A interfaces but with higher crystallinity are beneficial for higher *Voc* values, which can be one of the very important reasons for the high *Voc* of Por-Rod-based OSCs fabricated with pyridine and then thermal-annealed.

It is also worthy to note that **Por-Rod**-based devices show not only an extremely low energy loss to 0.53 eV but also a good J_{sc} up to 12.39 mA/cm^2, which can be confirmed by the EQE as shown in Figure 3b. The EQE of **Por-Rod**–based solar cells processed with pyridine additive and then thermal annealing exhibits a broad photo response from 300 to 850 nm with the maximum EQE value up to 61% at 520 nm and other two peak values over 50%, indicating it is possible to further enhance the efficiency by reducing the E_{loss} while maintaining high EQE

Journal of Materials Chemistry C Accepted Manuscript

This journal is © The Royal Society of Chemistry 20xx

Please do not adjust margins

values. To the best of our knowledge, the EQE up to 61% is the highest for the BHJ OSCs with an E_{loss} less than 0.55 eV. And the high EQE can be partially ascribed to the efficient exciton dissociation, which is demonstrated by photoluminescence (PL) quenching experiments.[43] As seen in Figure S3, **Por-Rod** pristine film exhibits PL emission peak at 805 nm, and it is quenched almost completely by $PC_{71}BM$ in the blend films, which suggests the efficient exiton separation. And the very weak PL of the blends is further quenched when processed with Py or Py+TA, indicating that more efficient exciton dissociation occurs in the active layers.

Table 2. Summary of device performances for **Por-Rod and Por-CNRod**

Molecule	Conditions	J_{sc} (mA/cm^2)	V_{OC} (V)	FF (%)	PCE (%)
Por-Rod	w/o	0.81	0.73	25.19	0.15
	Py[a]	1.44	0.86	22.35	0.28
	TA[b]	0.94	0.74	25.84	0.18
	Py+TA	12.39	0.94	42.71	4.97
Por-CNRod	w/o	0.72	0.87	19.68	0.12
	Py	2.43	0.94	26.39	0.60
	TA	0.37	0.81	21.09	0.06
	Py+ TA	1.37	0.89	26.79	0.33

[a] 1 v% pyridine, [b] thermal annealing at 100 ℃.

Hole-Mobility Measurement

The hole and electron mobilities of the blend films under different conditions shown in Figure 5, Figure S1 and Table S1 were estimated according to the electric-field dependent space charge limited current (SCLC) model in the configuration of ITO/PEDOT:PSS (40 nm)/active layer (85 nm)/MoO_3 (10 nm)/Ag (~60 nm) using the following equation:

$$J = \frac{9}{8}\varepsilon_r\varepsilon_0\frac{E^2}{d}\mu_0\exp\left(\beta\sqrt{E}\right)$$

Where J is the current, ε_r is the relative permittivity of the material, ε_0 is the permittivity of free space, E is the effective electric field, d is the thickness of the active layer, μ_0 is the zero-field mobility and β is the field activation factor.

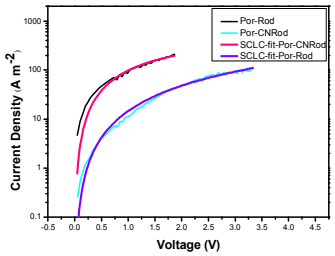

Figure 5. *J–V* characteristics of the hole-only devices in the configuration of ITO/PEDOT:PSS/active layer/MoO_3/Al.

Compared with those of pure chlorobenzene processed thin films, the electron mobility decreased to the half and hole mobility increased by five times for the bends fabricated with pyridine additive. However, thermal annealing and thermal annealing after adding pyridine lead to obvious improvements in hole and electron mobilities compared with processing with pyridine, which can be an important reason for the increase of FF and J_{sc}. The other reason is the smaller μ_h/μ_e ratio than that of the devices fabricated with Py and TA. Also, The SCLC hole mobilities of **Por-Rod** and **Por-CNRod** blend films with $PC_{71}BM$ under Py+TA condition are calculated to be 8.5×10^{-5} and 7.5×10^{-6} cm^2 V^{-1} s^{-1}, respectively. The higher hole mobility of **Por-Rod** can be one of the reasons why **Por-CNRod**-based devices show the higher J_{sc} because a higher mobility usually lead to a smaller photocurrent loss caused by charge recombination.

Morphology Characterizations

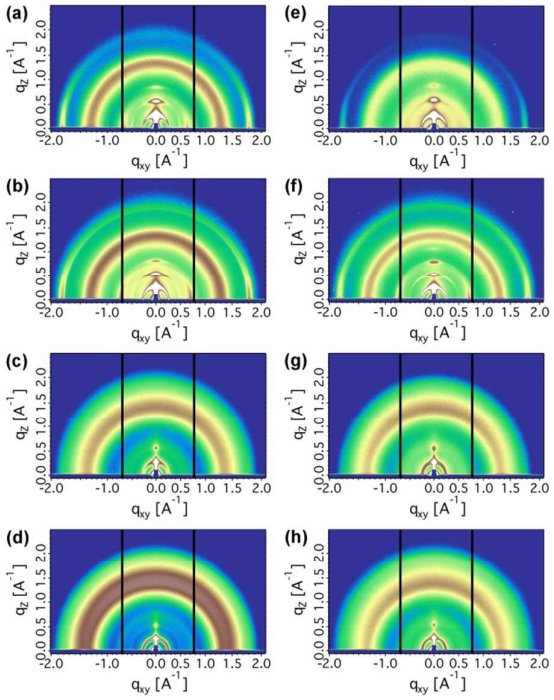

Figure 6. GIXD of **Por-Rod** and **Por-CNRod** in BHJ blends. (a, e) as spun from CB; (b, f) thermal annealed film casted from CB; (c, g) thin film casted from CB+Py mixture; (d, h) thermal annealed films from CB+Py processing.

The structure order of these materials in BHJ blends was studied by grazing incidence X-ray diffraction (GIXD) methods. Showing in Figure 5 are the GIXD images. From the as casted thin films from CB, it is quite obvious that **Por-Rod** and **Por-CNRod** take an edge-on orientation. Quite sharp (100) diffraction peak is seen from out-of-plane direction, accompanied with 3-4 high ordered reflections. Strong π-π stacking peak shows up in in-plane directions, with a wide angle spreading of intensities. Thus the orientation of crystallites is poor.[47] The detailed line-cut profiles are summarized in Figure 6. For **Por-Rod** blends, the π-π stacking peak located at 1.84 A^{-1}, giving a distance of 3.41 Å. This distance is quite small for organic semiconductor, which should be resulted from the porphyrin ring induced stacking. The (100) stacking located at 0.26 A^{-1}, corresponding to a 24.16 Å

Journal of Materials Chemistry C Accepted Manuscript

lamellae distance. It should be noted that in our previous studies that porphyrin and DPP based molecules are quite weak in molecule packing, even without obvious π-π stacking signal.[7] The modification in chemical structure, replacing the DPP moiety with thiophene and rhodanine, leads to stronger intermolecular packing. The crystal size is estimated using Scherr equation. The (100) crystal size is estimated to be 15.64 nm, and the π-π stacking peak is estimated to be 5.97 nm. For **Por-CNRod**, (100) distance is estimated to be 22.14 Å (located at 0.28 A^{-1}), π-π stacking distance is estimated to be 3.46 Å (located at 1.82 A^{-1}). Thermal annealing of as casted BHJ thin film leads to shifting of (100) peaks, which is more server in **Por-CNRod** blends. The (100) peak shifted to 0.24 A^{-1}, a ~2 Å distance shifting. The π-π stacking peak shifted to 1.86 A^{-1}; the size is also increased about 9.67, corresponding to ~3 layer of π stacks. When pyridine is used in thin film processing, the nanostructure of BHJ thin film changed completely. Both (100) and π-π stacking peak became much less intensive and crystal size is largely reduced because pyridine is quite effective in reducing the crystallinity of porphyrin based materials due to the coordination with the metal center, which will strongly retard the molecular assembly. The subsequent thermal annealing does not help to improve the structure order of the BHJ thin film. Quite similar GIXD results are obtained.

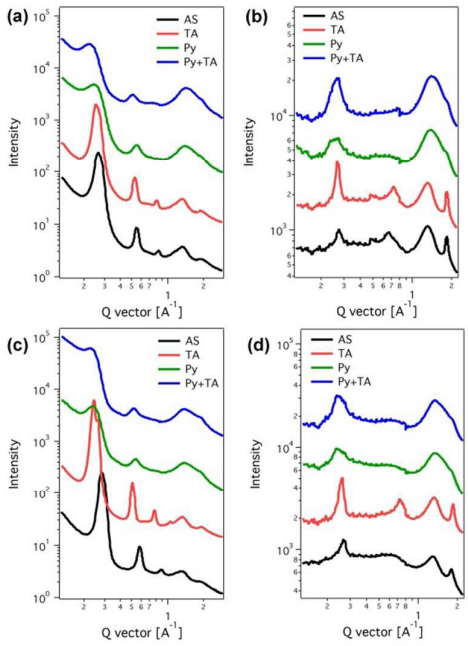

Figure 7. Line-cut profiles of GIXD results. (a) out-of-plane line cut of **Por-Rod** blends; (b) in-plane line cut of **Por-Rod** blends; (c) out-of-plane line cut of **Por-CNRod** blends; (d) in-plane line cut of **Por-CNRod** blends.

The length scale of phase separation was studied by using resonant soft X-ray scattering methods (RSoXS) by taking advantage of high scattering contrast at the carbon k-edges. For both **Por-Rod** and **Por-CNRod** blends, the as-cast samples show a quick decay of scattering signals in the very low q region, indicating a large scale phase separation outside of the probing length scales. Thermal annealing does not generate new length scale of phase separation and a nearly identical morphology is seen in this system. When pyridine additive is used, a small length scale of phase separation at ~20 nm (0.032 A^{-1}) is seen for **Por-Rod** blends. Further thermal annealing leads to enhancement of this scattering peak at an even larger q positions, corresponding to a length scale of ~16 nm (0.039 A^{-1}). This new scattering feature can be the critical of enhancing the device performance, giving a much larger short circuit current and power conversion efficiency. For **Por-CNRod** blends, using pyridine as the additive do lead to a smaller length scale of phase separation showing a peak at 0.025 A^{-1} with low scattering intensities. Further thermal annealing does not improve this length scale of phase separation. A quite similar scattering profile is recorded. From morphological aspects, it should be concluded that both **Por-Rod** and **Por-CNRod** blends processed from pyridine additive and the subsequent thermal annealing should lead to improved device performances. The low lying LUMO energy level of **Por-CNRod**, which cannot align well with PCBM, can be a major issue to efficiently split excitons and generate current.

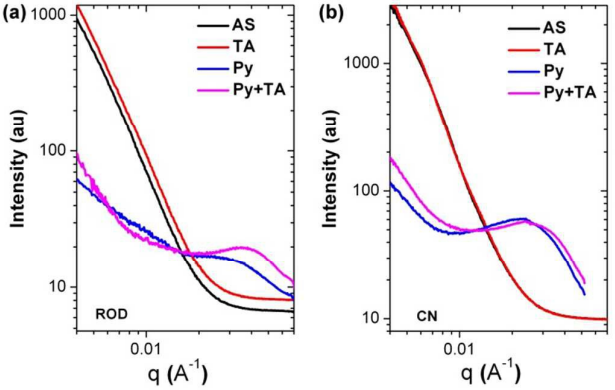

Figure 8. RSoXS of (a) **Por-Rod** blends; (b) **Por-CNRod** blends.

Conclusions

In summary, two new conjugated A-D-A porphyrin small molecules of **Por-Rod** and **Por-CNRod** are designed and synthesized through Sonogashira reactions. The BHJ OSCs based on the two porphyrins and $PC_{71}BM$ as the active materials in a conventional device structure under different conditions were investigated, and the **Por-Rod**-based devices processed with pyridine additive and then thermal annealing exhibit a PCE up to 4.97% with a V_{OC} of 0.94 V and a maximum EQE up to 61%. The energy loss for **Por-Rod**-based devices is only 0.53 eV which can compare to perovskite solar cells, and this is the first report that such low energy loss BHJ OSCs can exhibit EQE values more than 60%. However, **Por-CNRod**-based OSCs show very poor performance under the investigated condition even though a very low energy loss of only 0.51 eV has been recorded. Morphology studies using GIXD and RSoXS show that while pyridine additive reduces the crystallinity of porphyrin and the length scale of phase

Journal of Materials Chemistry C Accepted Manuscript

This journal is © The Royal Society of Chemistry 20xx

Please do not adjust margins

separation, the subsequent thermal annealing leads to the enhancement of the scattering peak corresponding to an even smaller length scale, which can be critical for the enhanced performance of **Por-CN**–based devices. The morphology of **Por-CNRod** blends is quite similar with that of **Por-CN** blends under the same fabrication conditions, and the low lying LUMO energy level of **Por-CNRod**, which cannot align well with PCBM to efficiently split excitons and generate current, can be a major issue for the poor performance of all the **Por-CNRod-**based OSCs. The results provide a further understanding of the energy loss and help to design new donors with high V_{OC} values for more efficient organic solar cells.

Acknowledgements

This work was financially supported by grants from International Science & Technology Cooperation Program of China (2013DFG52740, 2010DFA52150) and National Natural Science Foundation of China (51473053, 51073060). K Gao and L Xiao contributed equally to this work. Portions of this research were carried out at beamline 7.3.3 and 11.0.1.2 at the Advanced Light Source, and Molecular Foundary, Lawrence Berkeley National Laboratory, which was supported by the DOE, Office of Science, and Office of Basic Energy Sciences.

Notes and references

1. A. Mishra and P. Baeuerle, *Angew. Chem. Int. Ed.*, 2012, **51**, 2020-2067.
2. Y. Lin, Y. Li and X. Zhan, *Chem. Soc. Rev.*, 2012, **41**, 4245-4272.
3. L. Yuan, Y. Zhao, J. Zhang, Y. Zhang, L. Zhu, K. Lu, W. Yan and Z. Wei, *Adv. Mater.*, 2015, **27**, 4229-4233.
4. J. L. Wang, Q. R. Yin, J. S. Miao, Z. Wu, Z. F. Chang, Y. Cao, R. B. Zhang, J. Y. Wang, H. B. Wu and Y. Cao, *Adv. Funct. Mater.*, 2015.
5. B. Kan, M. Li, Q. Zhang, F. Liu, X. Wan, Y. Wang, W. Ni, G. Long, X. Yang, H. Feng, Y. Zuo, M. Zhang, F. Huang, Y. Cao, T. P. Russell and Y. Chen, *J. Am. Chem. Soc.*, 2015, **137**, 3886-3893.
6. W. Ni, M. Li, F. Liu, X. Wan, H. Feng, B. Kan, Q. Zhang, H. Zhang and Y. Chen, *Chem. Mater.*, 2015, **27**, 6077-6084.
7. K. Gao, L. Li, T. Lai, L. Xiao, Y. Huang, F. Huang, J. Peng, Y. Cao, F. Liu, T. P. Russell, R. A. Janssen and P. Xiaobin, *J. Am. Chem. Soc.*, 2015, **137**, 7282-7285.
8. Y. Sun, J. Seifter, L. Huo, Y. Yang, B. B. Hsu, H. Zhou, X. Sun, S. Xiao, L. Jiang and A. J. Heeger, *Adv. Energy Mater.*, 2015, **5**, 1400987.
9. D. Liu, M. Xiao, Z. Du, Y. Yan, L. Han, V. Roy, M. Sun, W. Zhu, C. S. Lee and R. Yang, *J. Mater. Chem. C*, 2014, **2**, 7523-7530.
10. Z. Du, W. Chen, Y. Chen, S. Qiao, X. Bao, S. Wen, M. Sun, L. Han and R. Yang, *J. Mater. Chem. A*, 2014, **2**, 15904-15911.
11. Y. Chen, Y. Yan, Z. Du, X. Bao, Q. Liu, V. Roy, M. Sun, R. Yang and C. S. Lee, *J. Mater. Chem. C*, 2014, **2**, 3921-3927.
12. K. Sun, Z. Xiao, S. Lu, W. Zajaczkowski, W. Pisula, E. Hanssen, J. M. White, R. M. Williamson, J. Subbiah, J. Ouyang, A. B. Holmes, W. W. H. Wong and D. J. Jones, *Nature communications*, 2015, **6**.
13. M. Cheng, C. Chen, X. Yang, J. Huang, F. Zhang, B. Xu and L. Sun, *Chem. Mater.*, 2015, **27**, 1808-1814.
14. Z. Zheng, S. Zhang, M. Zhang, K. Zhao, L. Ye, Y. Chen, B. Yang and J. Hou, *Adv. Mater.*, 2015, **27**, 1189-1194.
15. H. Kang, S. Kee, K. Yu, J. Lee, G. Kim, J. Kim, J. R. Kim, J. Kong and K. Lee, *Adv. Mater.*, 2015, **27**, 1408-1413.
16. J. D. Chen, C. Cui, Y. Q. Li, L. Zhou, Q. D. Ou, C. Li, Y. Li and J. X. Tang, *Adv. Mater.*, 2015, **27**, 1035-1041.
17. Y. Liu, J. Zhao, Z. Li, C. Mu, W. Ma, H. Hu, K. Jiang, H. Lin, H. Ade and H. Yan, *Nature communications*, 2014, **5**, 5293.
18. Q. Zhang, B. Kan, F. Liu, G. Long, X. Wan, X. Chen, Y. Zuo, W. Ni, H. Zhang, M. Li, Z. Hu, F. Huang, Y. Cao, Z. Liang, M. Zhang, T. P. Russell and Y. Chen, *Nat. Photonics*, 2015, **9**, 35-41.
19. C. Cui, X. Guo, J. Min, B. Guo, X. Cheng, M. Zhang, C. J. Brabec and Y. Li, *Adv. Mater.*, 2015, DOI: 10.1002/adma.201503815.
20. C. D. Wessendorf, G. L. Schulz, A. Mishra, P. Kar, I. Ata, M. Weidelener, M. Urdanpilleta, J. Hanisch, E. Mena‐Osteritz and M. Lindén, *Adv. Energy Mater.*, 2014, **4**, 201400266.
21. V. Gupta, A. K. K. Kyaw, D. H. Wang, S. Chand, G. C. Bazan and A. J. Heeger, *Sci. Rep.*, 2013, **3**, 1965.
22. F. C. Krebs, N. Espinosa, M. Hosel, R. R. Sondergaard and M. Jorgensen, *Adv. Mater.*, 2014, **26**, 29-39.
23. Y. Sun, G. C. Welch, W. L. Leong, C. J. Takacs, G. C. Bazan and A. J. Heeger, *Nat. Mater.*, 2012, **11**, 44-48.
24. N. J. Jeon, J. H. Noh, W. S. Yang, Y. C. Kim, S. Ryu, J. Seo and S. I. Seok, *Nature*, 2015, **517**, 476-480.
25. Q. Hu, J. Wu, C. Jiang, T. Liu, X. Que, R. Zhu and Q. Gong, *ACS nano*, 2014, **8**, 10161-10167.
26. B. Walker, C. Kim and T.-Q. Nguyen, *Chem. Mater.*, 2011, **23**, 470-482.
27. J. E. Coughlin, Z. B. Henson, G. C. Welch and G. C. Bazan, *Accounts Chem. Res.*, 2013, **47**, 257-270.
28. W. Li, K. H. Hendriks, A. Furlan, M. M. Wienk and R. A. Janssen, *J. Am. Chem. Soc.*, 2015, **137**, 2231-2234.
29. M. Wang, H. Wang, T. Yokoyama, X. Liu, Y. Huang, Y. Zhang, T. Q. Nguyen, S. Aramaki and G. C. Bazan, *J. Am. Chem. Soc.*, 2014, **136**, 12576-12579.
30. D. Veldman, S. C. J. Meskers and R. A. J. Janssen, *Adv. Funct. Mater.*, 2009, **19**, 1939-1948.
31. Z. Xiao, C. Bi, Y. Shao, Q. Dong, Q. Wang, Y. Yuan, C. Wang, Y. Gao and J. Huang, *Energ. Environ. Sci.*, 2014, **7**, 2619-2623.
32. Q. Peng, Q. Huang, X. Hou, P. Chang, J. Xu and S. Deng, *Chem. Commun.*, 2012, **48**, 11452-11454.
33. P. K. Nayak, G. Garcia-Belmonte, A. Kahn, J. Bisquert and D. Cahen, *Energ. Environ. Sci.*, 2012, **5**, 6022-6039.
34. Y. Lu, Z. Xiao, Y. Yuan, H. Wu, Z. An, Y. Hou, C. Gao and J. Huang, *J. Mater. Chem. C*, 2013, **1**, 630-637.
35. L. Koster, S. E. Shaheen and J. C. Hummelen, *Adv. Energy Mater.*, 2012, **2**, 1246-1253.
36. H. Qin, L. Li, F. Guo, S. Su, J. Peng, Y. Cao and X. Peng, *Energy Environ. Sci.*, 2014, **7**, 1397-1401.
37. Y. Huang, L. Li, X. Peng, J. Peng and Y. Cao, *J. Mater. Chem.*, 2012, **22**, 21841-21844.

Journal of Materials Chemistry C Accepted Manuscript

Please do not adjust margins

38. Y. I. H. Chao, J.-F. Jheng, J.-S. Wu, K.-Y. Wu, H.-H. Peng, M.-C. Tsai, C.-L. Wang, Y.-N. Hsiao, C.-L. Wang, C.-Y. Lin and C.-S. Hsu, *Adv. Mater.*, 2014, **26**, 5205-5210.
39. Q. Zhang, B. Kan, F. Liu, G. Long, X. Wan, X. Chen, Y. Zuo, W. Ni, H. Zhang and M. Li, *Nat. Photonics*, 2015, **9**, 35-41.
40. B. Kan, M. Li, Q. Zhang, F. Liu, X. Wan, Y. Wang, W. Ni, G. Long, X. Yang and H. Feng, *J. Am. Chem. Soc.*, 2015, **137**, 3886-3893.
41. Z. Li, G. He, X. Wan, Y. Liu, J. Zhou, G. Long, Y. Zuo, M. Zhang and Y. Chen, *Adv. Energy Mater.*, 2012, **2**, 74-77.
42. S. Chen, L. Xiao, X. Zhu, X. Peng, W.-K. Wong and W.-Y. Wong, *Chem. Commun.*, 2015, **51**, 14439-14442.
43. C. V. Kumar, L. Cabau, E. N. Koukaras, A. Sharma, G. D. Sharma and E. Palomares, *J. Mater. Chem. A*, 2015, **3**, 16287-16301.
44. S. Loser, C. J. Bruns, H. Miyauchi, R. P. Ortiz, A. Facchetti, S. I. Stupp and T. J. Marks, *J. Am. Chem. Soc.*, 2011, **133**, 8142-8145.
45. H. Zhou, L. Yang and W. You, *Macromolecules*, 2012, **45**, 607-632.
46. D. M. Guldi, *Chem. Commun.*, 2000, 321-327.
47. R. Fitzner, E. Mena-Osteritz, A. Mishra, G. Schulz, E. Reinold, M. Weil, C. Körner, H. Ziehlke, C. Elschner, K. Leo, M. Riede, M. Pfeiffer, C. Uhrich and P. Bäuerle, *J. Am. Chem. Soc.*, 2012, **134**, 11064-11067.

Journal of Materials Chemistry C Accepted Manuscript

This journal is © The Royal Society of Chemistry 20xx

TOC:

Solution-processed bulk heterojunction solar cells based on porphyrin small molecules with very low energy losses comparable to perovskite solar cells and high quantum efficiencies

Ke Gao[a], Liangang Xiao[a], Yuanyuan Kan[a], Binglin Yang[a], Junbiao Peng[a], Yong Cao[a], Feng Liu*[b], Thomas Russell[c] and Xiaobin Peng*[a]

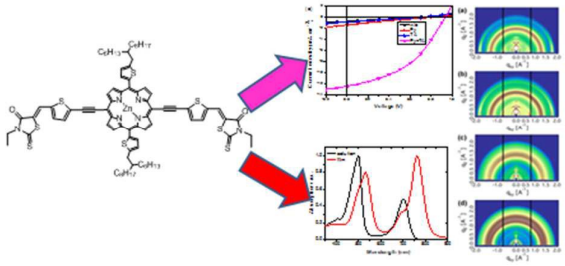

The BHJ OSCs show an energy loss of 0.53 eV but a maximum external quantum efficiency up to 61%.

Journal of Materials Chemistry C Accepted Manuscript